Photocatalytic Removal of Dye and Reaction Mechanism Analysis over Y_2O_3 Composite Nanomaterials

Xiaohui Guo[1,a], Jinyan Liu[1] and Guibao Guo[1]

[1]*School of Chemistry and Chemical Engineering, Inner Mongolia University of Science & Technology, Baotou 014010, Inner Mongolia, China*

Abstract. Y_2O_3 supported photocatalysts MOx (M=Fe, Ti and Bi)/Y_2O_3 were synthesized by hydrothermal and deposition-precipitation method and used in photocatalytic degradation of xylenol orange and rhodamine B under UV light irradiation. The crystalline structure and optical properties were well characterized by XRD and UV-vis DRS. The results of XRD revealed that the MOx/Y_2O_3 were composed of Fe_2O_3, TiO_2, $Bi_{0.8}Y_{1.2}O_3$ and Y_2O_3. The UV-vis DRS showed that MOx/Y_2O_3 photocatalysts exhibited stronger absorption in ultraviolet, and the absorption edge shifted to visible light region significantly. The photocatalytic experiments indicated that MOx/Y_2O_3 photocatalysts showed better activity for photodegradation of xylenol orange than rhodamine B. Moreover, the role of Y_2O_3 and the mechanism of photocatalysis is proposed.

1 Introduction

Rare earth (RE) elements are extensively exploited in metallurgical machinery, petroleum chemical industry, glass-ceramics, agriculture and functional materials due to their unique optical, electrical, magnetic and catalytic properties. However, the imbalance exploitation of RE elements severely restricted the development of RE industry, especially the overcapacity of light RE elements Ce, La and Y, so it is very important to tackle the application of light RE elements. Light RE elements as catalysts or catalytic components has been widely applied in petroleum chemical industry, catalytic combustion of fossil fuels, automotive emissions control, the purification of industrial waste air, and solid solution fuel cells [1] and showed excellent performance, that was ascribed to be one of the most effective way of application and foreground.

Photocatalysis is a promising technology for solving energy and environmental issues. In most of rare earth oxides, CeO_2 has been successfully used as photocatalysts to degrade sewage and pollutants because of its strong redox properties of Ce^{3+}/Ce^{4+} and the formation of oxygen vacancies [2, 3]. While La and Y only acted as dopant in photocatalysts, such as La/Y doped TiO_2 [4-6], Y_2O_3-ZnO [7], Y doped graphene oxide [8] and La_2O_3-Bi_2O_3 [9], had been synthesized to photocatalytic degradation of dye wastewater. The major role of RE ions in doped photocatalysts is supposed to enhance electron-hole pairs separation, improve optical absorption properties, modify adsorption capacity of dye and increase surface concentration of adsorbed OH group [10-13]. Nonetheless, the mechanism and active species of Y doped photocatalysts has not been thoroughly studied.

[a] Corresponding author : gxhsxicc@163.com

In this work, Y_2O_3 supported photocatalysts were synthesized via hydrothermal and deposition-precipitation method. XRD and UV-vis diffuse reflectance spectra were carried out to characterize the crystalline structure and optical property. The photocatalytic activity was tested by degradation of xylenol orange (XO) and rhodamine B (RhB) aqueous solutions under UV light irradiation. The photocatalytic mechanism is proposed based on the band potential analysis and active species trapping experiment.

2 Experimental

2.1 Catalyst preparation

All chemical reagents were of analytical grade and used without further purification. MO_x/Y_2O_3 supported photocatalysts were synthesized by two-step (hydrothermal and deposition-precipitation) process. Firstly, Y_2O_3 support was prepared as follows: 2 mmol $Y(NO_3)_3 \cdot 6H_2O$ was dissolved in 20 mL of deionized water, and then 60 mL KOH aqueous solution (5 mol/L) was added into the solution to form white precipitation. After being magnetically stirred for 1 h, the mixture was transferred into a 100 mL Teflon-lined autoclave which was subsequently heated at 180 ^oC for 12 h. After cooling down to room temperature, the solid products were filtered, washed with deionized water, dried at 60 ^oC overnight, calcined at 500 ^oC for 5 h, and finally Y_2O_3 powder was obtained.

Secondly, MO_x/Y_2O_3 photocatalysts were prepared by deposition-precipitation methods. Typically, 0.2 g of the as-prepared Y_2O_3 powder was dispersed in 20 mL of deionized water and sonicated for 30 min, and then desired amount of 20 mL of $Fe(NO_3)_3 \cdot 9H_2O$ aqueous solution was added. The suspension was magnetically stirred for 30 min and 40 mL of K_2CO_3 solution (0.5 mol/L) was added under vigorous stirring for 3 h. Subsequently, the mixtures were filtered, washed with deionized water, dried at 60 ^oC overnight, calcined at 500 ^oC for 2 h, and finally FeO_x/Y_2O_3 samples were obtained. Bi_2O_3/Y_2O_3 sample was synthesized by analogous procedure, except that $Bi(NO_3)_3 \cdot 5H_2O$ was dissolved in 5 mL of 1 mol/L HNO_3 solution. While TiO_2/Y_2O_3 sample was prepared as follow: 0.3 ml of tetrabutyl titanate was added into 80 ml of ethanol solution containing 0.2 g of Y_2O_3 powder and sonicated for 30 min to form mixture A, and then 1 ml $NH_3 \cdot H_2O$ (25%-28%) was added dropwise into A to make titanium source hydrolyze accompanying with continuously stirring at room temperature for 3 h. The resulting mixture dried by rotary evaporation at 80 ^oC, calcined at 500 ^oC for 2 h, and finally the product was denoted as TiO_2/Y_2O_3. The weight contents of MO_x in all of MO_x/Y_2O_3 photocatalysts were 25 %.

2.2 Characterization

Powder X-ray diffraction profiles were performed on Bruker D8 ADVANCE diffractometer at a scanning rate of 5^o/min in the 2θ range from 20^o to 80^o, with Cu Kα radiation (λ=1.5406 Å) at 40 kV and 40 mA. Diffuse reflectance spectra (DRS) were carried out on Agilent Cary 100 UV-vis spectrophotometer in the range of 200-800 nm using $BaSO_4$ as reference.

2.3 Photocatalytic activity

The photocatalytic activity of all samples was evaluated toward photodegradation of xylenol orange (XO) and rhodamine B (RhB) aqueous solutions under UV light irradiation (8 W, λ=365 nm). In details, 100 mL suspension containing 0.2 g/L of catalyst and 20 mg/L of XO or RhB was sonicated for 5 min, magnetically stirred in dark for 1 h to ensure an adsorption-desorption equilibrium, and then irradiated under UV light. Simultaneously, at given intervals, small aliquots of suspension were sampled and centrifuged to remove catalysts. The XO or RhB concentrations in filtrates were analyzed on UV-vis spectrophotometer (Analytik Jena, SPECORD 50) in the range of 200-700 nm using H_2O as reference.

The process of active species trapping experiments is the same as photocatalytic tests; besides, ascorbic acid (AA, 0.1 mmol/L), triethanolamine (TEOA, 0.01 mol/L) and t-butanol (TBA, 0.01 mol/L) were added to dye solution to trap the superoxide radicals ($\cdot O_2^-$), holes (h^+) and hydroxyl radicals (·OH), respectively.

3 Results and discussion

3.1 Characterization of catalysts

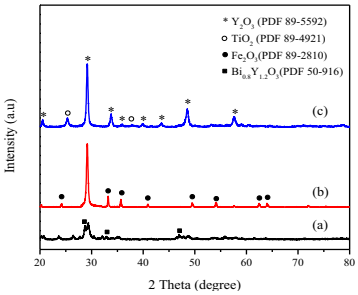

Figure 1. XRD patterns of MO_x/Y_2O_3 samples (a) Bi_2O_3/Y_2O_3, (b) Fe_2O_3/Y_2O_3, (c) TiO_2/Y_2O_3

Fig.1 shows the XRD patterns of MO_x/Y_2O_3 photocatalysts. For Bi_2O_3/Y_2O_3 (Fig.1a), two sets of XRD peaks of cubic Y_2O_3 (PDF 89-5592) and cubic $Bi_{0.8}Y_{1.2}O_3$ (PDF 50-916) were observed. Compared with Fe_2O_3/Y_2O_3 and TiO_2/Y_2O_3 samples, the intensity of diffraction peaks ascribed to Y_2O_3 dramatically decreased indicating the low degree of crystallinity, this is because Y_2O_3 can partly dissolve in HNO_3 and precipitate with Bi^{3+} together in the process of preparation. For Fe_2O_3/Y_2O_3 and TiO_2/Y_2O_3 samples (Fig.1b and c), the support YO_3 is indexed to cubic structure of Y_2O_3 (PDF 89-5592), its diffraction peak shape is irrelevant to loaded metals (Fe or Ti), and the second components can be indexed to hematite α-Fe_2O_3 (PDF 89-2810) and anatase TiO_2 (PDF 89-4921), respectively.

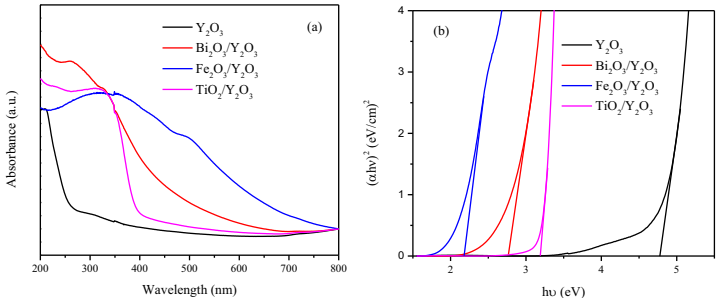

Figure 2. UV-vis absorbance spectra (a) and plot of $(\alpha h\nu)^2$ versus hν (b) of MO_x/Y_2O_3 samples

The UV-vis diffuse reflectance spectra (DRS) of Y_2O_3 and MO_x/Y_2O_3 photocatalysts were displayed in Fig.2. Taking pure Y_2O_3 support for comparison, supported MO_x/Y_2O_3 photocatalysts exhibited stronger absorption in ultraviolet, and the absorption edge shifted to visible light region significantly, especially for Fe_2O_3/Y_2O_3, which is responsive to visible light nearly to 800 nm. Moreover, Bi_2O_3/Y_2O_3 possessed strongest absorption in UV range indicating more active species (·OH) produced on the surface of sample [7].

The band gaps (E_g) of MO_x/Y_2O_3 composites were calculated from following equation [14]: $\alpha h\nu = A(h\nu - E_g)^{n/2}$, where α, ν, E_g and A are the absorption coefficient, light frequency, band gap, and a constant, respectively; n depends on the characteristics of transition in a semiconductor, n is 4 for direct band gap and 1 for indirect band gap. Y_2O_3 is indirect band gap, so n is equal to 1 [15]. Fig.2b shows the plot of $(\alpha h\nu)^2$ vs energy ($h\nu$) for MO_x/Y_2O_3 composites, the E_g can be obtained by

extrapolating the linear portion of the curve or tail. Compared to pure Y_2O_3 (4.76 eV), TiO_2/Y_2O_3, Bi_2O_3/Y_2O_3 and Fe_2O_3/Y_2O_3 samples possess E_g of 3.2, 2.8 and 2.2 eV, respectively, representing potential photocatalytic applications under visible light irradiation. The remarkable red shift of UV-vis DRS and reduction in E_g of those three supported samples were due to the fact that absorption spectral lines in Fig.2a are the superposition of each individual component. Coupling effectively promote the separation of photogenerated electrons and holes between two composite materials, but don't change their own band gaps. Consequently, the calculated band gap in this work should be attributed to TiO_2, Bi_2O_3 and Fe_2O_3, respectively, and well coincide with the values in Ref. [16].

3.2 Photocatalytic activity

Fig.3 reveals the photodegradation activity of XO and RhB in the presence of MO_x/Y_2O_3 photocatalysts, and the inset of figure is the structure of XO and RhB. For photodegradation of XO, TiO_2/Y_2O_3 and Fe_2O_3/Y_2O_3 samples showed faster photocatalytic rate in the early 90 min. As time increased further, the photodegradation rate of Bi_2O_3/Y_2O_3 sample increased rapidly and exceeded that of Fe_2O_3/Y_2O_3 sample. Fig.3a shows that the photodegradation of XO obeys the pseudo-first-order decay kinetics, the rate was illustrated as following formula: $ln(C_0/C)=k_{app}\cdot t$, where k_{app} is the apparent rate constants (min^{-1}). Plotting $ln(C_0/C)$ *vs*. t gives k_{app} from slope of linear fit, and keeps linear regression values R^2>0.97. The k_{app} were found to be 0.0102, 0.0105 and 0.0120 min^{-1} for Fe_2O_3/Y_2O_3, Bi_2O_3/Y_2O_3 and TiO_2/Y_2O_3, respectively, implying TiO_2/Y_2O_3 sample have the best photocatalytic activity.

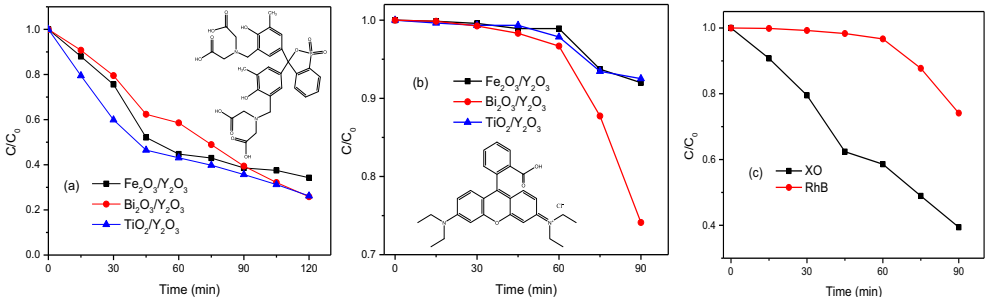

Figure 3. Photodegradation performance of (a) XO, (b) RhB over MO_x/Y_2O_3, and (c) comparison of photodegradation activity over Bi_2O_3/Y_2O_3 catalyst. (20 mg of catalyst, 100 mL of XO/RhB aqueous solution 20 mg/L)

Whereas for photodegradation of RhB, the photodegradation rate of three samples increased very slowly in 60 min, then raised approximately linearly in the last 30 min, and Bi_2O_3/Y_2O_3 sample performed the highest activity within 90 min. Nevertheless, all of three samples showed very low activity for photodegradation of RhB compared to photodegradation of XO, this was seen obviously in Fig.3c. The activity difference between XO and RhB might be derived from their molecular structure difference. From inset of Fig.3a and b, XO with four carboxylmethyl groups are more apt to be adsorbed on alkaline surface and subsequently photodegraded by photocatalysts than RhB that has only one carboxyl group. Further, the anion Cl^- in RhB is detrimental to photodegradation reaction owing to scavenging of active sites [17].

3.3 Postulated mechanism

To illustrate the photocatalytic mechanism of MO_x/Y_2O_3 and explain the origin of active species, the role of Y_2O_3 was analyzed. Y_2O_3, as a basic oxide, is abundant with surface hydroxyl and adsorbed oxygen [18], and that facilitates the photocatalytic oxidation of dye. On the other hand, coupling of band gaps between Y_2O_3 and MO_x should be taken into account.

The relative positons of valence band (VB) and conduction band (CB) edges was calculated as following [19, 20]: $E_{CB} = \chi - E_e - 0.5 \cdot E_g$ and $E_{VB} = E_{CB} + E_g$, where E_{CB} and E_{VB} are the CB and VB edge potential, χ is the absolute electronegativity, E_e is the energy of free electrons at the hydrogen scale (about 4.5 eV), E_g is the band gap. The calculated E_{VB} and E_{CB} were listed in Table 1.

Table 1. Absolute electronegativity (χ), Band gap (E_g), energy levels of calculated conduction band edge (E_{CB}) and valence band edge (E_{VB}) with respect to normal hydrogen electrode (NHE) for metal oxides.

Metal oxide	X (eV)	E_g (eV)	E_{CB} (eV)	E_{VB} (eV)
Bi_2O_3	6.23	2.8	0.33	3.13
TiO_2	5.81	3.2	-0.29	2.91
Fe_2O_3	5.88	2.2	0.28	2.48
Y_2O_3	5.35	4.76	-1.53	3.23

The case of Fe_2O_3/Y_2O_3 and TiO_2/Y_2O_3 were analogous to Bi_2O_3/Y_2O_3, so Bi_2O_3/Y_2O_3 was analyzed in detail. Bi_2O_3 was excited by UV light and generated electrons and holes pairs (Eq.(1)), but they don't transfer to Y_2O_3 owing to the mismatch of CB and VB edge potential between Y_2O_3 and Bi_2O_3. On the other side, the CB potential (0.33 eV) [16] of Bi_2O_3 is positive than $E(O_2/\cdot O_2^-)$ (-0.13 eV *vs*. NHE) [8], therefore, the electrons on the CB of Bi_2O_3 don't reduce adsorbed O_2 to $\cdot O_2^-$. The VB potential (3.13 eV) [16] of Bi_2O_3 is positive than $E(OH^-/\cdot OH)$ (1.89 eV *vs*. NHE) [8], and thus the holes on the VB of Bi_2O_3 can oxidized OH^- to $\cdot OH$.

Although the band potential of Y_2O_3 don't couple with that of Bi_2O_3, Y^{3+} was supposed to act intermediate for photogenerated electrons and holes pairs separation, where Y^{3+} acts as electron-acceptor (electron-trap) and electron-donor (hole-trap) to inhibit recombination of charge pairs and is reduced/oxidized to Y^{2+}/Y^{4+} individually (Eq.(2, 3)) [12]. Subsequently, the unstable Y^{2+} and Y^{4+} can release trapped e^-/h^+ pairs through Eq. (4, 5) and produce active species $\cdot O_2^-$ and $\cdot OH$. The $\cdot O_2^-$ may further react to from $\cdot OH$ (Eq.(6)).

$$Bi_2O_3 + h\nu \rightarrow e^- + h^+ \quad (1)$$
$$Y^{3+} + h^+ \rightarrow Y^{4+} \text{ (hole trap)} \quad (2)$$
$$Y^{3+} + e^- \rightarrow Y^{2+} \text{ (electron trap)} \quad (3)$$
$$Y^{2+} + O_2(ads) \rightarrow Y^{3+} + \cdot O_2^- \quad (4)$$
$$Y^{4+} + OH^-(ads) \rightarrow Y^{3+} + \cdot OH(ads) \quad (5)$$
$$\cdot O_2^- + e^- + 2H^+ \rightarrow H_2O_2 \rightarrow \cdot OH + OH^- \quad (6)$$
$$XO + (\cdot O_2^-, \cdot OH) \rightarrow \text{Degradation products} \quad (7)$$

There are many works explored the photocatalytic active species on various photocatalysts. Chen [21] reported that $\cdot OH$ was the main active species for RhB degradation on flower-like $Bi_2O_2CO_3$, while Peng [22] suggested that h^+ and $\cdot O^{2-}$ are the main active species in RhB photodecomposition under solar light irradiation on WO_3-Bi_2WO_6.

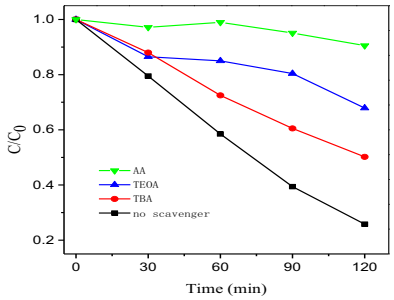

Figure 4. Effect of scavenger on photodegradation performance of XO aqueous solution over Bi_2O_3/Y_2O_3.

(20 mg catalyst, 20 mg/L of XO aqueous solution, 100 mL, 120 min)

In order to discriminate the active species in this work, the trapping experiments were carried out as before mentioned. Fig.4 shows the impact of different scavengers on the photodegradation efficiency over Bi_2O_3/Y_2O_3 sample. It is observed that the addition of AA dramatically decreased

photodegradation activity, the degradation efficiency of XO declined from 74.1 % to 9.5 % (120 min). The addition of TEOA and TBA reduced degradation efficiency of XO to 32.1% and 49.8 %, respectively. These results suggest that $\cdot O_2^-$ and ·OH are both important for photodegradation of XO over Bi_2O_3/Y_2O_3 sample under UV light irradiation (Eq.(7)).

4 Conclusions

In summary, MO_x (M=Fe, Ti and Bi)/Y_2O_3 supported photocatalysts have been successfully synthesized by hydrothermal and deposition-precipitation method. They exhibited stronger absorption in ultraviolet, the absorption edge shifted to visible light region significantly, and E_g was largely reduced with respect to pure Y_2O_3. TiO_2/Y_2O_3 and Bi_2O_3/Y_2O_3 samples showed the highest activity for photodegradation of XO and RhB, respectively. The major role of Y_2O_3 is to enhance the OH^- concentration on the surface of photocatalysts, and Y^{3+} performed synergistic effects to trap charge pairs and inhibit e^-/h^+ recombination. The $\cdot O_2^-$ and ·OH are the main active species for photocatalytic degradation of XO over Bi_2O_3/Y_2O_3 sample.

Acknowledgments

The authors are grateful for the financial support provided by the Natural Science Foundation of Inner Mongolia of China (Grant No. 2014BS0204), Scientific Research Program in University of Inner Mongolia of China (Grant No. NJZY14163).

References

1. W. C. Zhan, Y. Guo, X. Q. Gong, Y. C. Guo, Y. Q. Wang, G. Z. Lu, Chin. J. Catal. 35, 1238 (2014)
2. N. S. Arul, D. Mangalaraj, T. W. Kim, P. C. Chen, N. Ponpandian, P. Meena, Y. Masuda, J. Mater Sci: Mater Electron. 24, 1614 (2013)
3. T. Feng, X. D. Wang, G. S. Feng, Mater. Lett. 100, 36 (2013)
4. Y. J. Wang, L. J. Jiang, C. G. Feng, Desalin. Water Treat. 52, 4802 (2014)
5. M. Meksi, G. Berhault, C. Guillard, H. Kochkar, Catal. Comm. 61, 107 (2015)
6. D. M. Tobaldi, R. C. Pullar, A. S. Škapin, M. P. Seabra, J. A. Labrincha, Mater. Res. Bull. 50, 183 (2014)
7. T. M. Su, Z. Z. Qin, H. B. Ji, Y. X. Jiang, Int. J. Photoenergy. doi:10.1155/2014/794057 (2014)
8. Y. Zhang, S. S. Yuan, Y. H. Zhao, H. G. Wang, C. D. He, J. Mater. Chem. A. 2, 7897 (2014)
9. H. Q. Deng, T. Tang, C. H. Fu, Q. Y. Jiang, Y. M. Hu, J. C. Huo, Environ. Sci. Technol. 36, 121 (2013)
10. S. Z. Chen, S. M. Xu, G. Xu, L. Y. Li, Rare Metal Mat. Eng. 35, 505 (2006)
11. L. Y. Lin, M. H. Yeh, C. Y. Chen, R. Vittal, K. C. Ho, J. Mater. Chem. A. 2, 8281 (2014)
12. A. N. Ökte, Ö. Yilmaz, Appl. Catal. B: Environ. 85, 92 (2008)
13. C. J. Hao, J. Li, Z. L. Zhang, Y. J. Ji, H. H. Zhan, F. X. Xiao, D. Wang, B. Liu, F. B. Su, Appl. Surf. Sci. 331, 17 (2015)
14. C. Saranyoo, I. Burapat, W. Khatcharin, Mater. Res. Bull. 54, 28 (2014)
15. P. K. Patel, K. L. Yadav, Physica B. 442, 39 (2014)
16. Y. Xu, M. A. A. Schoonen, Am. Mineral. 85, 543 (2000)
17. D. Kanakaraju, C. A. Motti, B. D. Glass, M. Oelgemöller, Chemosphere. 139, 579 (2015)
18. L. H. Zhao, X. M. Zheng, J. H. Fei, Chin. J. Catal. 17, 227 (1996)
19. M. A. Ahmed, E. E. EI-Katori, Z. H. Gharni, J. Alloys Compd. 553, 19 (2013)
20. H. Tian, F. Teng, J. Xu, S. Q. Lou, N. Li, Y. X. Zhao, M. D. Chen, Sci. Rep. 5, 7770 (2015)
21. L. Chen, R. Huanag, S. F. Yin, S. L. Luo, C. T. Au, Chem. Eng. J. 193-194, 123 (2012)
22. Y. Peng, Q. G. Chen, D. Wang, H. Y. Zhou, A. W. Xu, Cryst. Eng. Comm. 17, 569 (2015)